SEARS FOUNDATION FOR MARINE RESEARCH
Yale University

Journal of Marine Research

Volume 25, Number 3

On the Theory of Continental Shelf Waves[1]

Lawrence A. Mysak

Pierce Hall, Harvard University
Cambridge, Massachusetts

ABSTRACT

This paper considers the response of the sea surface to a low-frequency long-wavelength plane-wave pressure distribution that progresses eastward across a large circular continent having a narrow sloping shelf that drops off vertically to a flat ocean basin. Using the linearized inviscid shallow-water equations for a homogeneous uniformly rotating fluid, it is shown that the sea level on the shelf and in the deep-sea regions generally responds as an inverse barometer. However, for certain small frequency bands, the response on the shelf is not inverse barometric. In this case the forcing frequency excites an eigenfrequency of the system, and the shelf sea level consists of the superposition of two waves: (i) an eastward-moving plane wave and (ii) a nondispersive circularly traveling wave (continental shelf wave) that moves counterclockwise in the southern hemisphere and clockwise in the northern hemisphere. Also determined are the changes in the shelf-wave phase velocity due to a continental slope region and deep-sea stratification and current that flows alongside the shelf.

1. *Introduction.* When a static normal-stress distribution acts upon the sea surface, the sea level reacts as an inverse barometer, or "barometrically".[2] In the past this has also been assumed to be the case when the distribution is time-dependent, as in ordinary moving weather systems, provided the fluctuations are of sufficiently low frequency (considerably less than the Coriolis

1. Accepted for publication and submitted to press 8 April 1967.

2. In the literature, such a response is often called "isostatic" (for example, see Hamon 1966); however, in this paper the term "barometric" is used.

parameter). Recently, however, Hamon (1962, 1966) and Hamon and Hannan (1963) have observed that the daily mean sea-level fluctuations on the Australian coast are not barometric: at four stations on the eastern coast the behavior was appreciably less than barometric. (That is, the magnitude of the "barometric factor," or ratio of daily mean sea level changes to atmospheric pressure changes, is appreciably less than the expected value of 1.0 cm/mb.) However, at two stations on the western coast the behavior was appreciably greater than barometric. On the other hand, an analysis of a simultaneous record of the daily mean sea-level fluctuations at Lord Howe Island has indicated a barometric behavior.

Another unexpected phenomenon observed by Hamon (1962, 1963, 1966) is the existence of time lags in the adjusted sea level between neighboring coastal stations whose separation is of the order of 100 km. (The adjusted sea level is defined as the observed sea level with the atmospheric pressure eliminated according to the hydrostatic relation 1-cm decrease in sea level for 1-mb increase in pressure.) More specifically, for a series of six east-coast stations between Eden (37°S) and Urangan (25°S), the lags between adjacent stations are related in a manner that suggests the presence of a northward-traveling wave having a speed of about 400 cm/sec. On the other hand, the lagged correlations between adjusted sea levels at the west coast stations Geraldton, Fremantle, and Bunbary suggest the presence of a southward-traveling wave. In this case the wave speed has not been determined accurately, but it has been estimated to be in the range of 300 to 600 cm/sec.

Robinson (1964) has theoretically established that there are low-frequency long-wavelength surface waves that travel parallel to a straight continental boundary. For the topography of the sea bottom in the vicinity of the continent, he employed a uniformly sloping shelf that drops off vertically to deep water of constant depth. He found that these waves, which he termed "continental shelf waves," are essentially confined to the shelf and depend very strongly on the Coriolis parameter. But, they are not truly Rossby waves, since Robinson has treated the Coriolis parameter as a constant; nor are they edgewaves (Munk et al. 1956, Greenspan 1956, Reid 1958) for the following reasons: (i) the decay of the shelf-wave amplitude occurs in the deep-sea region, (ii) in a specified hemisphere, the waves can propagate in only one direction along the coast, (iii) the waves are nondispersive, and (iv) the waves have a very low frequency (considerably less than the Coriolis parameter). Furthermore, these waves are characterized by a hydrostatic balance in the vertical direction and by a nearly geostrophic balance in the direction normal to the coast; however, in the direction along the coast, the geostrophic terms and the local acceleration are of the same order of magnitude. Robinson has also shown that when shelf waves are excited by a northward-traveling plane-wave pressure distribution, a nonbarometric behavior on the eastern Australian coast occurs, provided the forcing frequency lies within a small neighborhood of

an eigenfrequency. Finally, he showed that, on the eastern Australian shelf, the waves travel northward, and the lowest-mode wave moves with a speed of 250 cm/sec, which is of the order of the observed wave speed in this region. However, because Robinson has dealt with a straight infinite coastline, his forced solution does not yield any information about the variation in sea-level behavior with latitude. Second, his solution does not indicate whether shelf waves are also excited by the generally eastward-moving weather systems that progress across Australia.

To obtain for the Australian continent a more realistic geometry that will yield the latitudinal dependence of the sea-level behavior, and in order to answer the question raised at the end of the above paragraph, first consideration in this paper is given to the following problem: the response of the sea surface to a plane-wave pressure distribution that progresses eastward across a circular continent having a uniformly sloping shelf that drops off vertically to water of constant depth. For this model, it is shown in § 2 that the sea level over the shelf and in deep-sea regions generally responds barometrically. However, for certain small frequency bands, the response on the shelf is not barometric. In that case the shelf sea level consists of the superposition of two waves: (i) an eastward-traveling plane wave and (ii) a nondispersive circularly traveling shelf wave that moves counterclockwise in the southern hemisphere and clockwise in the northern hemisphere. The above theory, when applied to the Australian stations, where an anomalous sea-level behavior has been observed (§ 3), does in general predict the observed behavior, provided the forcing frequency lies in a small neighborhood of an eigenfrequency. However, the theoretical lowest-mode wave speeds for the eastern and western coasts of Australia are somewhat less than the observed. In § 4 it is shown that, if the geometry of the model considered in § 2 is modified so as to include a finite-slope continental slope region, the wave speeds are significantly increased. For the eastern and western coasts of Australia, the increase in the lowest-mode wave speeds is about 30%. While there is now good agreement between the theoretical and observed wave speeds for the west coast, there is still a significant discrepancy for the east coast. In view of the fact that the theory does not take into account the intense current and associated stratification that is present off the eastern Australian coast (Hamon 1965, CSIRO Australia 1963), this discrepancy is perhaps not too surprising. In § 5 the change in wave speeds due to deep-sea stratification (idealized by a two-layer model) and a uniform upper-layer deep-sea current that flows alongside the shelf is determined.

2. *Formulation of Problem and its Solution.* Equation for the Adjusted Sea Level. Let the center of the continent be the origin of a cylindrical polar coordinate system (r, ψ, z), with z measured vertically upward and r, ψ measured in the usual manner. Furthermore, let ζ be the sea-level distortion

and $\emptyset$ the negative of the atmospheric-pressure fluctuations measured in centimeters of water. Let $\emptyset$ have the form of an eastward-moving plane wave,[3] viz.,

$$\emptyset = \emptyset_0 \exp\left[i(kr\cos\psi - \omega t)\right],$$

where $\emptyset_0$ and k are assumed to be constant. In terms of ζ and $\emptyset$, the adjusted sea level, η, which is a measure of the deviation of the sea-level behavior from exact barometric behavior, is given by $\eta = \zeta - \emptyset$. In terms of the above notation, the linearized nondissipative equations of shallow-water theory for a uniformly rotating homogeneous fluid imply that $\eta(r, \psi)$ satisfies the equation

$$\begin{aligned} rh\nabla^2\eta + h'(r\eta_{,r} + if\omega^{-1}\eta_{,\psi}) - r(f^2-\omega^2)g^{-1}\eta = \\ = r(f^2-\omega^2)g^{-1}\emptyset_0 \exp(ikr\cos\psi), \end{aligned} \tag{2.1}$$

where $z = -h(r)$ is the equation of the sea bottom, f the Coriolis parameter (assumed constant), and g the acceleration of gravity (for details, see Mysak 1966). In the derivation of (2.1) it has been assumed that η and u_r, u_ψ (the horizontal velocity components) have a time dependence of the form $\exp(-i\omega t)$. Finally, in terms of $\eta(r,\psi)$, $u_r(r,\psi)$ and $u_\psi(r,\psi)$ are given by

$$u_r(r,\psi) = g(i\omega\eta_{,r} - fr^{-1}\eta_{,\psi})/(f^2-\omega^2), \tag{2.2}$$

$$u_\psi(r,\psi) = g(f\eta_{,r} + i\omega r^{-1}\eta_{,\psi})/(f^2-\omega^2), \tag{2.3}$$

provided $\omega^2 \neq f^2$.

For the circular geometry described in § 1, $h(r)$ takes the form

$$h = \begin{cases} D, r > R+l & \text{(deep-sea region)}, \\ d(r-R)/l,\ R < r < R+l & \text{(shelf region)}, \end{cases}$$

where D is the depth in the deep-sea region, d the depth at the edge of the shelf, l the shelf width, and R the continental radius. Eq. (2.1) is to be solved separately in the deep-sea and shelf regions subject to the boundary conditions $|\eta(R,\psi)| < M$ (a constant) and $\eta(\infty,\psi) = 0$. At the edge of the shelf, η and $u_r h$ (radial transport component) are stipulated to be continuous.

In (2.1), (2.2), and (2.3), we assume that $\omega^2 \ll f^2$. Hence, in the deep-sea region, (2.1) reduces to

$$(\nabla^2 - \beta^2)\eta = \beta^2\emptyset_0 \exp(ikr\cos\psi), \quad r > R+l, \tag{2.4}$$

where $\beta^2 = f^2/gD$. Upon examining the forcing term in (2.4), note that, for $r \sim k^{-1}$ and $\beta^2 \ll k^2$, $\eta = O(\beta^2\emptyset_0/k^2)$, which implies that in the deep-sea region the amplitude of η is generally much less than that of $\emptyset$, which indi-

3. The response of the sea surface to an arbitrary forcing function will be dealt with in a future paper.

cates a nearly barometric behavior. For $\varepsilon = l/R \ll 1$ and $\gamma = -fl/\omega R$, $\alpha = f^2 Rl/gd$, $\partial/\partial\xi$, and $\partial/\partial\psi$ each of order unity, eq. (2.1) in the shelf region reduces to

$$\xi\eta_{,\xi\xi} + \eta_{,\xi} - i\gamma\eta_{,\psi} = \varepsilon\alpha\emptyset_0 \exp(ikR\cos\psi), \quad 0 < \xi < 1, \tag{2.5}$$

where $\xi = (r - R)/l$. Hence $\eta = O(\varepsilon\alpha\emptyset_0/\gamma)$, which implies that the shelf sea-level behavior is also essentially barometric unless resonance occurs. The unforced equations obtained from (2.4) and (2.5), together with the above stated boundary and continuity conditions, constitute an eigenvalue problem with eigenvalue γ. Since $\gamma \propto \omega^{-1}$, it follows that, when the forcing frequency lies within a small neighborhood of an eigenfrequency, η on the shelf is amplified, thereby leading to a nonbarometric behavior.

Unforced Solution: Continental Shelf Waves. The appropriate solutions to (2.4) and (2.5), which are single-valued in ψ, are given by

$$\eta(r,\psi) = \begin{cases} \Sigma_m A_m K_m[\beta(l\xi + R)] \exp(im\psi), & \xi > 1, \\ \Sigma_m B_m \mathcal{J}_0[2(\gamma m\xi)^{1/2}] \exp(im\psi), & 0 < \xi < 1, \end{cases} \tag{2.6}$$

where $m = 0, \pm 1, \pm 2, \ldots$, K_m is the m^{th}-order modified Bessel function of the second kind and $\mathcal{J}_0$ the zeroth-order Bessel function of the first kind. Upon applying the continuity conditions to (2.6), it is found that $A_0 = B_0 = 0$ and the eigenvalue equation is obtained:

$$\begin{aligned} &\mathcal{J}_0[2(\gamma m)^{1/2}][1 - \Delta + \varepsilon(1+\varepsilon)\beta R K_m'/\gamma m K_m] - \\ &- \Delta(1+\varepsilon)(\gamma m)^{-1/2}\mathcal{J}_0'[2(\gamma m)^{1/2}] = 0 \quad (m \neq 0), \end{aligned} \tag{2.7}$$

where K_m and K_m' are evaluated at $\xi = 1$ and $\Delta = d/D$. For $\beta R K_m'/K_m$ and γm each of order unity, and $\varepsilon \ll 1$ and $\Delta \ll 1$, eq. (2.7) implies that the eigenvalues are essentially given by the zeros of $\mathcal{J}_0$. Let λ_{0j} $(j = 1, 2, \ldots)$ denote the roots of the eq. $\mathcal{J}_0(\lambda) = 0$; then, under the above approximations, the eigenfrequencies are given by

$$\omega_{j,m} = -4fl m/R\lambda_{0j}^2 \quad (m \neq 0). \tag{2.8}$$

Finally, in view of (2.8), the adjusted sea-level eigenfunctions can be written in the form

$$\eta_{j,m}(r,\psi,t) = \begin{cases} O(\Delta), & \xi > 1, \\ \mathcal{J}_0[2(\gamma_{0j} m\xi)^{1/2}] \exp[i(m\psi - \omega_{j,m}t)] + o(\Delta), & 0 < \xi < 1, \end{cases} \tag{2.9}$$

where γ_{0j} is defined by $2(\gamma_{0j} m)^{1/2} = \lambda_{0j}$.

The following properties of the unforced solution should be noted.

(i) Each eigenfunction, $\eta_{j,m}$, is in the form of a circularly traveling wave that is almost entirely confined to the shelf; hence we adopt the term "conti-

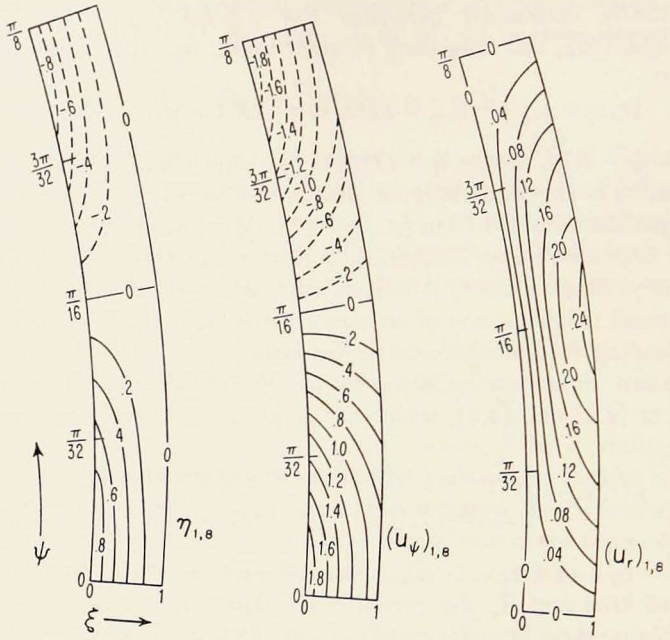

Figure 1. Contour lines of the shelf-wave field, $\eta_{1,8}$, and associated velocity fields over half a wavelength ($0 \leqslant \psi \leqslant \pi/8$) at the instant $t = 0$, corresponding to the case $l = 10^7$cm, $R = 2 \times 10^8$cm, and $f = -0.73 \times 10^{-4}$sec.$^{-1}$. Each field is shown for only half a wavelength, since η and u_ψ are even and u_r is odd in ψ. Since $f < 0$ in this example, these fields propagate counterclockwise around the shelf with constant angular velocity, $\omega_{1,8}/8$.

nental shelf waves" for the $\eta_{j,m}$'s. These waves correspond to Robinson's plane-traveling shelf waves. To within $O(\Delta)$, each wave has an antinode at the coast and a node at the edge of the shelf; for $j = 2, 3, \ldots$, the wave also has 1, 2, ... node(s) in the range $0 < \xi < 1$. The shelf-wave pattern $\eta_{1,8}$ [obtained by taking the real part of (2.9) with the term $O(\Delta)$ neglected] and associated shelf-current patterns [derived from (2.2) and (2.3)] at the instant $t = 0$ are shown in Fig. 1 for the range $0 \leqslant \psi \leqslant \pi/8$. Note that u_r is in quadrature with η and u_ψ, which are in phase, and that u_r is an order of magnitude smaller than u_ψ. In view of the latter result and the fact that ω is an order of magnitude smaller than f, the radial momentum equation implies that the waves are characterized by a nearly geostrophic balance of forces in the radial direction.

(ii) The eigenfrequencies, $\omega_{j,m}$, form a doubly discrete set. In the Cartesian geometry, the eigenfrequencies are given by $\omega_{j,k} = -4fl k/\lambda_{0j}^2$, where k is a N-S wave number that lies in the range $k^2 l^2 \ll 1$ (Robinson 1964). In the case of the circular geometry, it is clear that the effect of the periodicity requirement is to quantize the wave number, m.

(iii) In both geometries the waves are nondispersive and the phase velocity (wave speed) of the j^{th} mode is given by

$$c_j = -4fl/\lambda_{0j}^2. \tag{2.10}$$

In (2.10) note that the wave speed is proportional to the shelf width and is independent of the depth and acceleration of gravity, which is quite unlike the case for gravity waves and edgewaves. Furthermore, in the circular geometry observe that the waves travel counterclockwise in the southern hemisphere and clockwise in the northern hemisphere.

Note that continental shelf waves, though similar in form, are quite distinct from the well-known edgewaves (Munk et al. 1956, Greenspan 1956, Reid 1958). Edgewaves are dispersive, of a much higher frequency, are strictly confined to the shelf, and, in a specified hemisphere, can propagate in both directions along the shelf.

Forced Solution. To obtain the forced solution for the shelf, η is expanded in terms of the eigenfunctions given in (2.9), with $\omega_{j,m}$ in the exponent replaced by ω. The coefficients are then obtained from (2.5) upon employing the orthogonality relations for the eigenfunctions. To within $O(\Delta)$ it follows that the solution takes the form

$$\eta(\xi,\psi,t) = \varepsilon\alpha\mathcal{O}_0,\Sigma_{j,m}A_{j,m}\mathcal{J}_0[2(\gamma_{0j}m\xi)^{1/2}]\exp[i(m\psi-\omega t)],\ (m\neq 0), \tag{2.11}$$

where

$$A_{j,m} = i^m\mathcal{J}_m(kR)/(\gamma_{0j}m)^{1/2}\mathcal{J}_1[2(\gamma_{0j}m)^{1/2}]m(\gamma-\gamma_{0j}).$$

Eq. (2.11) explicity shows that, unless the forcing frequency, ω, lies within a "resonant" neighborhood of $\omega_{j,m}$ defined by

$$|m(\gamma-\gamma_{0j})| \lesssim \varepsilon\alpha|\mathcal{J}_m(kR)/(\gamma_{0j}m)^{1/2}\mathcal{J}_1[2(\gamma_{0j}m)^{1/2}]|, \tag{2.12}$$

the sea-level behavior on the shelf is nearly barometric. However, if ω lies within a resonant neighborhood of $\omega_{j,m}$, then η has an amplitude of $O(\mathcal{O})$, the leading contribution being $N_{j,m}$, the $(j,m)^{\text{th}}$ term of (2.11). In such a case the theoretical sea-level amplitude on the shelf is essentially given by $|\mathcal{O}+N_{j,m}|$. However, since the eigenfrequencies corresponding to $j = 2, 3, \ldots$, which are considerably less than the Coriolis parameter, have very large values of m and since $\mathcal{J}_m(kR)$ rapidly decreases with increasing m, the resonant neighborhood (2.12) will be largest for the eigenfrequencies corresponding to $j = 1$. Hence, an anomalous sea-level behavior on the shelf is essentially determined by $|\mathcal{O}+N_{1,m}|$, with ω within the resonant neighborhood of $\omega_{1,m}$ given by (2.12), with $j = 1$.

3. *Application of Theory to Australia.* In this section the theory developed in § 2 is applied to those regions of Australia where the observations on sea

level have been made by Hamon. To carry out this comparison between theory and observation, the origin of the coordinate system used in our model is taken to lie at Alice Springs, so that $f = -0.59 \times 10^{-4}$ sec^{-1} and $R = 2.05 \times 10^{8}$ cm. Furthermore, $d = 2 \times 10^{4}/$ cm and $D = 5 \times 10^{5}$ cm for the maximum shelf and average deep-sea depth and $l \equiv l_E = 5 \times 10^{6}$ cm and $l \equiv l_W = 7.5 \times 10^{6}$ cm, respectively, for the east-coast and west-coast shelf widths.

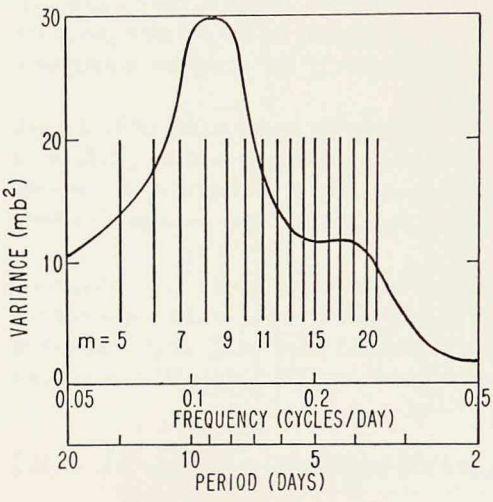

Figure 2. Winter spectrum of daily mean atmospheric pressure at Sydney, according to Hamon (1962). The vertical lines through the spectrum represent lowest-mode eigenfrequencies, $\omega_{1,m}$ ($m = 5,6,\ldots,20$) for $l = l_E$.

Fig. 2 represents the "winter" (April to September) power spectrum of the daily mean atmospheric pressure fluctuations at Sydney. In Fig. 2 the product of frequency and spectral energy density has been plotted against the logarithm of frequency; note that there exists a single, albeit broad, maximum at a period of 9 days. The winter spectrums for other midlatitude Australian stations computed by Hamon are similar to that shown in Fig. 1 and are also peaked at 9 days. On the other hand, during "summer" (October to March) the spectrums at the same stations are all peaked at a period of 5 days. It is well known that the ordinary weather systems over mid-Australia generally progress eastward. Hence the plane-wave driving force, $\emptyset$, used in the above theory is a fairly good approximation for the actual atmospheric pressure variations over mid-Australia, assuming that during winter (summer) the forcing frequency, ω, lies in a small neighborhood of $\omega_W = 0.81 \times 10^{-5}$ sec^{-1} ($\omega_S = 1.45 \times 10^{-5}$ sec^{-1}). In the expression for $\emptyset$, the wave number k, which is a measure of the E-W distance between mid-Australian anticyclonic centers, has the value $\pi \times 10^{-8}$ cm^{-1} (Karelsky, personal communication).

For the above values of $f, l, \omega, \ldots$, note that, when resonance does not occur, the behavior in the deep-sea and (eastern and western) shelf regions is barometric to within $O(10^{-2})$. Note also that the approximations made in developing the theory ($\omega^2 \ll f^2$, $l \ll R$, $d \ll D$, $\ldots$) introduce an error of only a few percent in so far as the case of Australia is concerned.

In considering the theoretical sea-level behavior at the eastern and western coasts of Australia, the following question arises. For a specified shelf width (l_E or l_W) and season (summer or winter), which $\omega_{1,m}$'s are most likely to be

excited? In Fig. 2 are plotted some of the eigenfrequencies, $\omega_{1,m}$, as given by (2.8), with $l = l_E$. For this case it is evident that $\omega_{1,8}$ and $\omega_{1,9}$ are most apt to be excited, since only these eigenfrequencies lie at the peak of the spectrum. For $l = l_W$, a similar analysis reveals that $\omega_{1,5}$ and $\omega_{1,6}$ are most likely to be excited. During summer, the eigenfrequencies most likely to be excited are $\omega_{1,14}$, $\omega_{1,15}$ for $l = l_E$, and $\omega_{1,9}$, $\omega_{1,10}$ for $l = l_W$.

To illustrate the coastal sea-level behavior in the neighborhood of the above specified eigenfrequencies, the normalized amplitude is used:

$$S_m \equiv |\mathcal{O} + N_{1,m}|_{\xi=0}/\mathcal{O}_0,$$
$$= \left\{1 + A_m^2 + 2A_m \cos\left[m\left(\psi + \frac{\pi}{2}\right) - kR\cos\psi\right]\right\}^{1/2}, \tag{2.13}$$

where

$$A_m = \varepsilon\alpha\mathcal{F}_m(kR)/0.62(m\gamma - 1.44).$$

When $S_m > 1$ or < 1, the sea-level behavior at the coast is respectively greater or less than barometric. When $A_m = O(1)$, note from (2.13) that the sea-level behavior does depend on ψ (as well as on m, ω, and l). Hence, it is not surprising that the observed Australian sea-level behavior at the eastern coast is quite different from that at the western coast. In Figs. 3–6 the amplitude S_m is plotted as a function of frequency for those east- and west-coast stations where an anomalous sea-level behavior has been observed during winter or summer or both. These stations are listed in Table I along with their observed behavior ($<$ and $>$ representing respectively a less or greater than barometric behavior) and position ψ. Note in Table I that the observed sea-level behavior during summer is less than barometric at each east-coast station and greater than barometric at each west-coast station; with the exceptions noted in Table I, the same statements apply to the winter sea-level behavior.

In Figs. 3–6, note the following:

(i) For both $l = l_E$ and $l = l_W$, the amplitude $S_m \to \infty$ as $\omega \to \omega_{1,m}+$ or $\omega \to \omega_{1,m}-$. This hypernonbarometric behavior at resonance arises because

Table I. Australian stations with observed anomalous sea-level behavior. No winter sea-level behaviors are available for Newcastle, Port Kembla, and Geraldton; hence, in the winter column these stations are marked with dashes.

		Position ψ	Observed behavior Winter	Summer
East Coast	Coff's Harbour	− 24°	<	<
	Newcastle	− 33°	−	<
	Sydney	− 37°	<	<
	Port Kembla	− 39°	−	<
West coast	Fremantle	−150°	>	>
	Geraldton	−161°	−	>

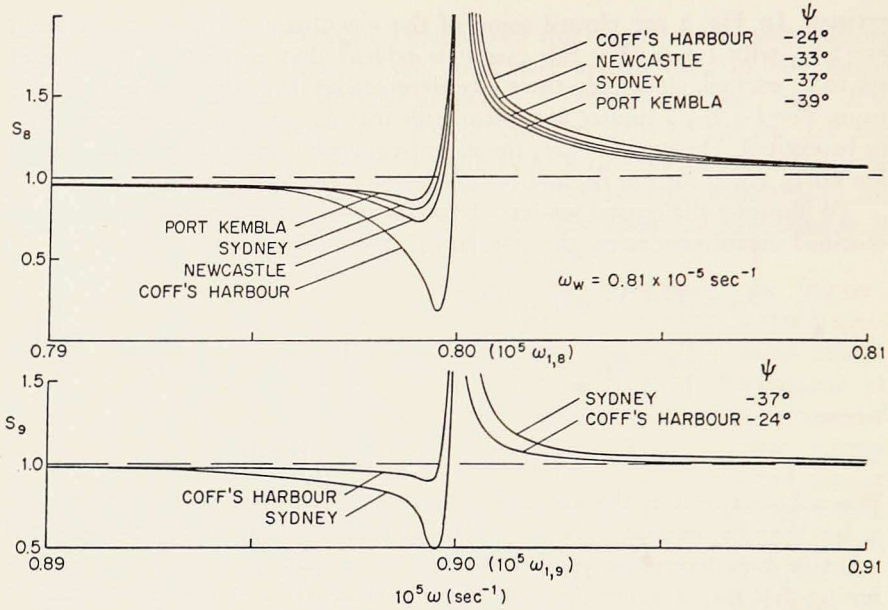

Figure 3. Undamped sea-level amplitude versus frequency in the neighborhood of eigenfrequencies $\omega_{1,8}$ (top) and $\omega_{1,9}$ (bottom) for shelf width $l = l_E$. The amplitudes S_9 for Port Kembla and Newcastle have been omitted, since they are nearly identical to S_9 for Sydney.

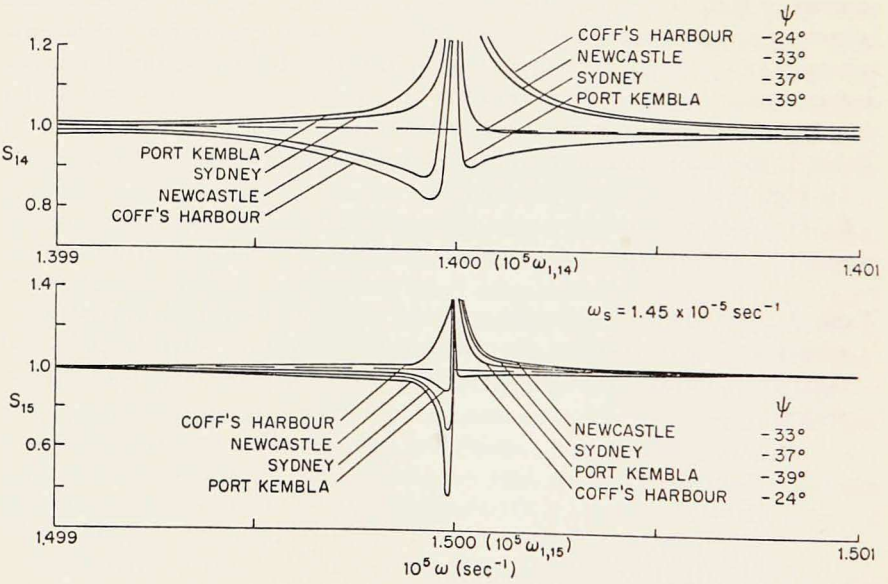

Figure 4. Undamped sea-level amplitude versus frequency in the neighborhood of eigenfrequencies $\omega_{1,14}$ (top) and $\omega_{1,15}$ (bottom) for shelf width $l = l_E$.

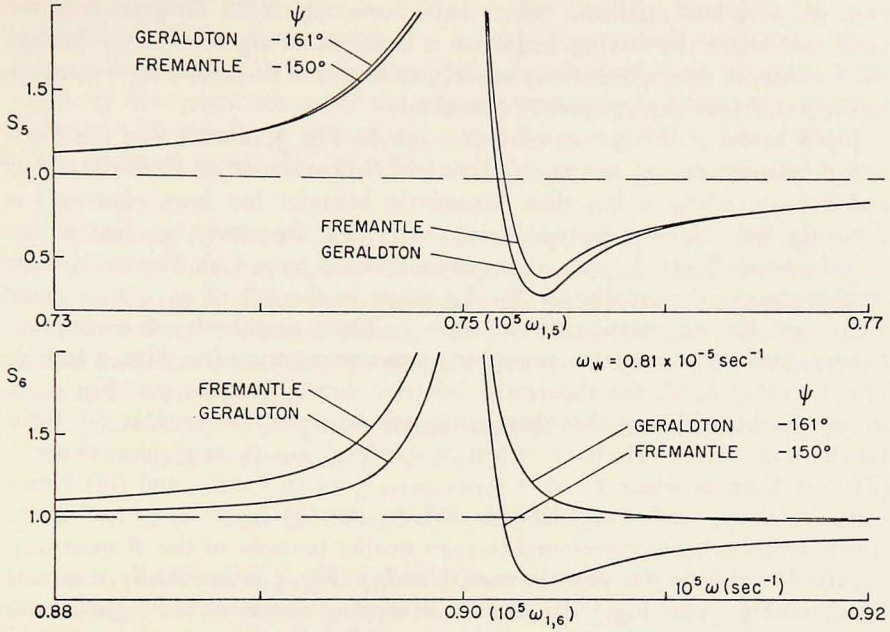

Figure 5. Undamped sea-level amplitude versus frequency in the neighborhood of eigenfrequencies $\omega_{1,5}$ (top) and $\omega_{1,6}$ (bottom) for shelf width $l = l_W$.

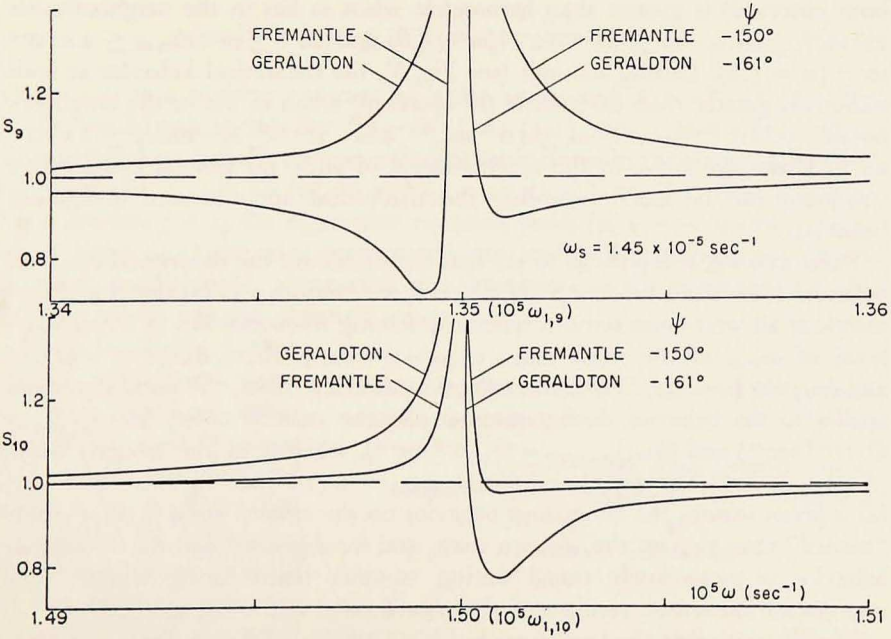

Figure 6. Undamped sea-level amplitude versus frequency in the neighborhood of eigenfrequencies $\omega_{1,9}$ (top) and $\omega_{1,10}$ (bottom) for shelf width $l = l_W$.

both diffusive and nonlinear effects have been neglected. To determine the amplitude when the forcing frequency is equal to an eigenfrequency (within the framework of a quasi-steady model), at least one of these effects must be incorporated into the equations of motion.

(ii) Behavior at the eastern coast ($l = l_E$). In Fig. 3, observe that the theoretical behavior during winter at all stations (in particular, at Coff's Harbour and Sydney, where a less than barometric behavior has been observed) is distinctly less than barometric when the forcing frequency, ω, lies in the neighborhoods $5\times10^{-9} \lesssim \omega_{1,m} - \omega \lesssim 2\times10^{-8}$ sec^{-1} ($m = 8,9$). For ω in these neighborhoods, the amplitudes S_m dip down to the left of $\omega_{1,m}$ to a value well below the barometric value of $S_m = 1$. These neighborhoods correspond to very small portions of the atmospheric pressure spectrum (see Figs. 2 and 3). On the other hand, the theoretical behavior during summer (see Fig. 4) is in agreement with the less-than-barometric-behavior observed at (i) New Castle and Coff's Harbour when $5\times10^{-10} \lesssim \omega_{1,14} - \omega \lesssim 3\times10^{-9}$ sec^{-1}, (ii) Port Kembla when $2\times10^{-10} \lesssim \omega - \omega_{1,14} \lesssim 2\times10^{-9}$ sec^{-1}, and (iii) Newcastle, Sydney, and Port Kembla when $10^{-10} \lesssim \omega_{1,15} - \omega \lesssim 10^{-9}$ sec^{-1}. These neighborhoods correspond to even smaller portions of the Φ spectrum.

(iii) Behavior at the western coast ($l = l_W$). Fig. 5 is essentially a mirror image of Fig. 3; in Fig. 5 the amplitude dipping occurs to the right of the eigenfrequencies. During winter the theoretical behavior at both stations (particularly at Fremantle, where a greater-than-barometric-behavior has been observed) is greater than barometric when ω lies in the neighborhoods $2\times10^{-8} \lesssim \omega_{1,m} - \omega \lesssim 10^{-7}$ sec^{-1} ($m = 5,6$) and $10^{-8} \lesssim \omega - \omega_{1,m} \lesssim 2\times10^{-8}$ sec^{-1} ($m = 5,6$). During summer (see Fig. 6), the theoretical behavior at both stations is greater than barometric (as observed) when ω lies in the neighborhoods $5\times10^{-9} \lesssim \omega_{1,10} - \omega \lesssim 10^{-8}$ sec^{-1} and $10^{-9} \lesssim \omega - \omega_{1,10} \lesssim 2\times10^{-9}$ sec^{-1}. However, for ω in the neighborhood of $\omega_{1,9}$, no general comparative statement can be made regarding the theoretical and observed anomalous behaviors.

Summarizing, it is possible to say that during winter the theoretical sea-level behavior is less than barometric at all east-coast stations and greater than barometric at all west-coast stations when the forcing frequency lies in a neighborhood of $\omega_{1,m}$ of the form $\delta\omega_2 < \omega_{1,m} - \omega < \delta\omega_1$, where $\delta\omega_1/\delta\omega_2 = O(10)$ and $\delta\omega_j > 0$ ($i = 1,2$). With the exception of a few cases, the same statement applies to the behavior during summer. At the eastern coast, $(\delta\omega_1)_{\text{winter}} = O(10^{-8}\text{ sec}^{-1})$ and $(\delta\omega_1)_{\text{summer}} = O(10^{-9}\text{ sec}^{-1})$, whereas at the western coast, $(\delta\omega_1)_{\text{winter}} = O(10^{-7}\text{ sec}^{-1})$ and $(\delta\omega_1)_{\text{summer}} = O(10^{-8}\text{ sec}^{-1})$. That is to say, for a given season, the anomalous behavior on the eastern coast is more finely "turned" than that on the western coast, and for a given coast, the anomalous behavior is more finely tuned during summer than during winter. The reasons for these two results are that $l_E < l_W$ and $\omega_W < \omega_S$, respectively.

Finally, note that the lowest-mode ($j = 1$) shelf wave travels counterclock-

wise with a speed given by $c_1 = -fl/1.44$ [see (2.10)]. Therefore, in the neighborhood of the eastern coast ($l = l_E$) this wave travels northward with speed $c_1 = 200$ cm/sec, which is about half the observed speed of 400 ± 100 cm/sec. In the neighborhood of the western coast ($l = l_W$), this wave travels southward with speed $c_1 = 310$ cm/sec, which lies just within the error bounds for the observed speed, viz., 300–600 cm/sec.

4. *Influence of Continental Slope.* If a finite-slope continental slope region is included in the theory of edgewaves, the wave speed is increased by about 2% (Munk et al. 1956). Since the wavelengths and periods associated with continental-shelf waves are much greater, it is quite plausible that a similar geometrical modification in our theory would give rise to an even larger increase in the shelf-wave speed.

For a uniformly sloping continental slope of width l', with depth d at $r = R + l$ and depth D at $r = R + l + l'$,

$$h(r) = (D-d)r/l' - (D-d)(R+l)/l' + d.$$

Note that, if $(D-d) \ll l'$, then $dh/dr \ll 1$, which is one of the underlying assumptions of shallow-water theory. Henceforth $(D-d) \ll l'$ is assumed. With the above form for h, it follows that, to within our order of approximations, the eigenvalues are given by

$$2(\gamma m)^{1/2} = \lambda_{0j} + q_j \Delta'^{1/2} \quad (m \neq 0; \quad j = 1,2,\ldots), \tag{4.1}$$

where $-q_j$ is a positive constant of order unity and $\Delta' = dl'/(D-d)l$ (for details, see Mysak 1966). For $l'/l = O(1)$, eq. (4.1) implies that a finite-slope continental-slope region produces a significant increase in the eigenfrequencies. For Australia, $l'_E = 7.5 \times 10^6$ cm and $l'_W = 12.5 \times 10^6$ cm. For these values of l' and the case $j = 1$, the eigenvalue equation yields $(q_1)_E = -0.9$ and $(q_1)_W = -1.1$. From (4.1) the new wave speeds are readily determined; the results are given in Table II, along with the theoretical values computed for the previous model and the observed values.

Note in Table I that, with a continental slope, the wave speed at either coast is increased by about 30%, which, as conjectured earlier, is much greater than the increase for edgewaves. The theoretical wave speed for the western coast now lies well within the error

Table II. Observed and theoretical lowest-mode wave speeds.

	Wave speed (cm/sec)		
	Theoretical		Observed
	without continental slope	with continental slope	
East coast	200	270	400 ± 100
West coast	310	410	300 – 600

bounds of the observed speed. For the eastern coast, however, the theoretical wave speed still lies outside the error bounds of the observed speed.

5. *Effect of Deep-sea Current and Stratification.* Two-layer Model with Current of Semi-infinite Width in Upper Layer. In this section the effect on the shelf-wave speeds of a very simple deep-sea current and stratification system is determined. Here use is made of the simpler Cartesian geometry employed by Robinson (1964), since a circular continental boundary itself does not yield any change in the wave speeds (see § 2). For a basic state (see Fig. 7), assume that there exists a uniform flow that moves parallel to the shelf but is confined to the deep-sea region and to an upper layer; in the deep-sea region below this upper layer lies a motionless fluid layer of slightly greater density. Upon this basic state is imposed a surface-wave motion parallel to the coast; this motion in turn induces a wave motion at the interface. If it is assumed that the basic current is geostrophic and baroclinic, then seaward the interface must slope downward. However, in the ensuing equations for the wave heights η and ζ', we make the simplifying approximation that the upper-layer and lower-layer depths are constant.

The intense current system (Hamon 1965) and associated deep-sea stratification (CSIRO Australia 1963) off the east Australian coast prompts consideration of this model. The main part of this current system, known as the East Australian Current (EAC), consists of a strong southerly flow (about 100–150 km in width) that moves alongside the shelf between 27°S and 37°S (that is, approximately between Coff's Harbour and Sydney). At the horizontal

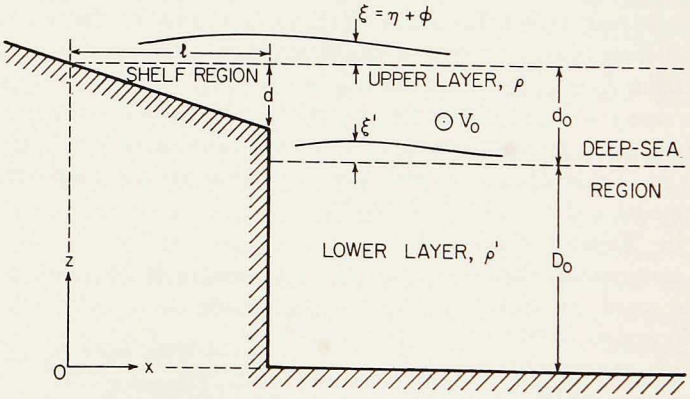

Figure 7. Cross-sectional diagram of two-layer model employed in the present analysis. The longshore coordinate, y, increases into the paper. The uniform basic flow, V_0, is in the negative y direction and is confined to the upper layer and to the deep-sea region. For the eastern Australian coast, typical values of V_0, d_0, ... are $V_0 = 100$ cm/sec, $d_0 = 2.5 \times 10^4$ cm, $D_0 = 5 \times 10^5$ cm, $l = 5 \times 10^6$ cm, $d = 2 \times 10^4$ cm, $\varrho = 1.025$ gm cm^{-3}, and $\varrho' - \varrho = 2.5 \times 10^{-3}$ gm cm^{-3}.

center of this current, the surface velocity reaches a maximum of about 100–150 cm/sec; the current velocity decreases progressively with depth so that at about 250 m the speed is about half of the surface velocity; below 250 m the velocity decreases more slowly with depth. From recent σ_t measurements (CSIRO Australia 1963) it is possible to infer that, in the vicinity of this southerly flow, the vertical density profile is well correlated with the depth profile of the current velocity. That is to say, the density increases rapidly with increasing depth to about 200–300 m and then increases very slowly with depth. The density difference between the upper and lower regions is approximately 2.5×10^{-3} gm cm^{-3}.

In terms of the notation shown in Fig. 7, the unforced linearized inviscid equations for (η,u,v) and (ξ',u',v') are given by

Shelf:

$$\left.\begin{aligned} u_t - fv + g\eta_x &= 0, \\ v_t + fu + g\eta_y &= 0, \end{aligned}\right\} \tag{5.1}$$

$$(hu)_x + hv_y + \eta_t = 0, \tag{5.2}$$

where $h = dx/l$.

Deep-sea:

upper layer:

$$\left.\begin{aligned} u_t - fv - V_0 u_x + g\eta_x &= 0, \\ v_t + fu - V_0 v_y + g\eta_y &= 0, \end{aligned}\right\} \tag{5.3}$$

$$d_0(u_x + v_y) - V_0(\eta - \xi')_y + (\eta - \xi')_t = 0, \tag{5.4}$$

lower layer:

$$\left.\begin{aligned} u'_t - fv' + g'\xi'_x + (\varrho/\varrho')g\eta_x &= 0, \\ v'_t + fu' + g'\xi'_y + (\varrho/\varrho')g\eta_y &= 0, \end{aligned}\right\} \tag{5.5}$$

$$D_0(u'_x + v'_y) + \xi'_t = 0. \tag{5.6}$$

In (5.5), the symbol g' denotes the reduced gravity and is related to g by the equation $g' = g(1 - \varrho/\varrho')$.

Note that, in the limit $g' \to 0 (\varrho' - \varrho \to 0)$, $V_0 \to 0$, $D_0 \to 0$, and $d_0 \to D$, the deep-sea equations (5.3)–(5.6) reduce to those used by Robinson (1964) for a homogeneous ocean of depth D without deep-sea current. However, with deep-sea stratification and current, the motion of η is coupled to that of ξ' [see (5.4) and (5.5)], so that new modes of oscillation for the system are expected.

To determine the eigenmodes for the system (5.1)–(5.6) together with appropriate boundary and continuity conditions, we first make the transformation $(\eta, u, v, \xi', u', v') = (N, X, Y, Z', X', Y') \exp[i(ky - \omega t)]$, where $N, X, \ldots$ are all functions of x alone. Then from (5.1)–(5.6) we obtain the following equations for the wave amplitudes N and Z':

Upper layer:

$$h(D^2-k^2)N+(Dh)(D-fk/\omega)N-[(f^2-\omega^2)/g]N=0, \quad 0<x<l, \tag{5.7}$$

$$d_0(D^2-k^2)N-[(f^2-\omega_0^2)/g](N-Z')=0, \quad x>l, \tag{5.8}$$

Lower layer:

$$D_0[g'(D^2-k^2)Z'+g(\varrho/\varrho')(D^2-k^2)N]-(f^2-\omega^2)Z'=0, \quad x>l. \tag{5.9}$$

Here $\omega_0=\omega+kV_0$ and $D=d/dx$. The boundary and continuity equations for the above system are as follows: for the upper layer, $|N(0)|<M$ (a constant), $N(\infty)=0$, and the N and x-component of the transport are to be made continous at $x=l$; for the lower layer, $X'(l)=0$ and $|Z'(\infty)|<M$ (a constant).

Assume that $\omega^2 \ll f^2$ and $\omega_0^2 \ll f^2$; hence, in (5.7)–(5.9) and in the expressions for X, Y, X', and Y', ω^2 and ω_0^2 are neglected. In (5.7), let $x=l\xi$; then, for $k^2l^2 \ll 1$ and $f^2l^2 \ll gd$, this equation reduces to

$$\left(\xi\frac{d^2}{d\xi^2}+\frac{d}{d\xi}+\varkappa\right)N=0,$$

where $\varkappa=-fkl/\omega$, which is the eigenvalue for the system; the above equation is identical to that derived by Robinson for the shelf-wave amplitude. The solution to the above equation that satisfies the condition at the coast is given by $A_s\mathcal{J}_0[2(\varkappa\xi)^{1/2}]$. In (5.8) and (5.9), let $\chi=kx$; then, after some rearrangement, these equations become

$$\begin{aligned}&\left[\frac{d^2}{d\chi^2}-(1+\alpha^2)\right]N+\alpha^2Z'=0, \quad 0<\chi<kl,\\ &\left(\frac{d^2}{d\chi^2}-1\right)N+\mu^2\left[\frac{d^2}{d\chi^2}-(1+\alpha'^2)\right]Z=0, \quad \chi>kl,\end{aligned} \tag{5.10}$$

where $\alpha^2=f^2/k^2gd_0$, $\alpha'^2=f^2/k^2g'D_0$, $\mu^2=(\varrho'-\varrho)/\varrho$. The solutions to (5.10), which satisfy the conditions at infinity, take the form

$$\begin{Bmatrix}N_j\\Z'_j\end{Bmatrix}=\begin{Bmatrix}A_j\\B_j\end{Bmatrix}\exp[-r_j(\chi-kl)] \quad (j=1,2; \quad r_j>0). \tag{5.11}$$

Hence, the following characteristic equation for r_j is obtained:

$$\mu^2r_j^4-\alpha^2(1+\varepsilon_1)r_j^2+\alpha^2(1+\varepsilon_2)=0, \tag{5.12}$$

where

$$\varepsilon_1=\mu^2(2+\alpha^2+\alpha'^2)/\alpha^2,$$

$$\varepsilon_2=\mu^2(1+\alpha^2)(1+\alpha'^2)/\alpha^2.$$

For $\alpha=O(1)$, $\alpha'=O(1)$, and $\mu^2 \ll 1$, note that $\varepsilon_1 \ll 1$ and $\varepsilon_2 \ll 1$. To a first order in small quantities, the positive roots of (5.12) are given by $(r_1, r_2)=$

$(\alpha/\mu, 1)$. Hence, from (5.11) and the first equation in (5.10), $B_1 = -(1/\mu^2)A_1$ and $B_2 = A_2$ to a first order in small quantities. Finally, the complete solution for N and Z' is given by

$$N = \begin{cases} A_8 \mathcal{J}_0[2(\varkappa\xi)^{1/2}], & 0 < x < l, \\ A_1 \exp[-(\alpha/\mu)(\chi - kl)] + A_2 \exp[-(\chi - kl)], & x > l \end{cases} \tag{5.13}$$

$$Z' = -(1/\mu^2)A_1 \exp[-(\alpha/\mu)(\chi - kl)] + A_2 \exp[-(\chi - kl)], \; x > l. \tag{5.14}$$

Applying the condition $X'(l) = 0$ to (5.13) and (5.14) yields $A_2 = 0$; application of the continuity conditions yields the eigenvalue equation

$$\mathcal{J}_0[2(\varkappa)^{1/2}][\beta^* \varkappa(1 - \Delta_0) - (1 + \varkappa R_0)\Delta_0^{1/2}] - \\ -\beta^* \Delta_0 (\varkappa)^{1/2} \mathcal{J}_0[2(\varkappa)^{1/2}] = 0, \tag{5.15}$$

where $\beta^* = \mu(gd)^{1/2}/(l|f|) = O(1)$, $\Delta_0 = d/d_0 = O(1)$, and $R_0 = -V_0/fl = o(1)$.

Note that, in the limit $\beta^* \to 0 (\varrho' - \varrho \to 0)$ and $R_0 \to 0 (V_0 \to 0)$, eq. (5.15) implies that the eigenvalues are given by the zeros of $\mathcal{J}_0$, in agreement with the unstratified case with no basic deep-sea current. However, with stratification and a deep-sea current, (5.15) implies that the eigenvalues are quite different, since β^*, Δ_0, and R_0 are each of order unity. As noted, the physical reason for this change in the eigenvalues is that the motion of the surface wave η in the deep-sea region is now coupled to that of the interfacial wave ξ' through the conservation equations. However, observe that the waves are still nondispersive and progress northward at the eastern coast of a continent that lies in the southern hemisphere.

In Fig. 8, the lowest-mode wave speed, $c_1 [= -4fl/\varkappa_1$, where $\varkappa_1$ is the lowest eigenvalue as determined by (5.15)], is plotted

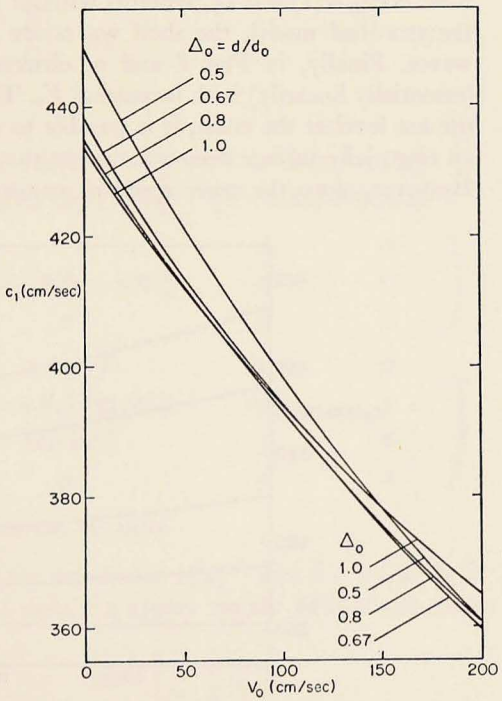

Figure 8. Theoretical shelf-wave speed of lowest eigenwave versus deep-sea current speed for $\varrho' - \varrho = 2.5 \times 10^{-3}$ gm cm^{-3} and various values of Δ_0.

as a function of V_0 for various values of Δ_0 for the case of the eastern Australian coast in the area from Sydney to Coff's Harbour ($f = -0.73 \times 10^{-4}$ sec^{-1}, $l = 5 \times 10^6$ cm). The higher eigenvalues and corresponding wave speeds have not been calculated in detail, since only the lowest-mode eigenwave has so far been observed. We only note that, for the special case $\Delta_0 = 1$ and $V_0 = 0$, $c_2 = 70$ cm/sec, which is considerably less than c_1 for these values of Δ_0 and V_0 (see Fig. 8).

In Fig. 8, observe that, for V_0 in the range 50–100 cm/sec (typical EAC speeds) and for all the values of Δ_0 considered, the theoretical lowest-mode wave speed now lies midway between the error bounds of the observed wave speed, viz., 400 ± 100 cm/sec. Even for $V_0 = 0$, note that c_1 still lies well within the error bounds for the observed speed. That is to say, the main shortcoming of the earlier models was the absence of deep-sea stratification. However, while the wave speeds are relatively insensitive to changes in the thickness of the upper layer (Fig. 8), they are quite sensitive to changes in the density difference between the two layers (Fig. 9). Note that, with stratification, the shelf-wave amplitude at the edge of the shelf is quite different from zero; now $N(0)/N(1) \approx 0.25$, whereas without stratification, $N(0)/N(1) \approx 0.04$. In the stratified model, the shelf waves are strongly coupled with the deep-sea waves. Finally, in Figs. 8 and 9, observe that, for $\varrho' - \varrho \neq 0$, c_1 decreases (essentially linearly) with increasing V_0. This result suggests that, by analyzing the sea level at the coast, it is possible to determine theoretically the speed of an essentially surface deep-sea current that flows alongside a continental shelf. However, since the wave speed in any small coastal section (distance of the

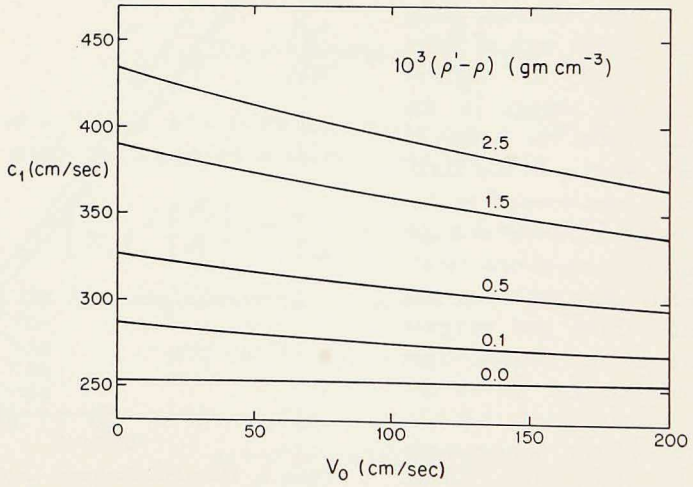

Figure 9. Theoretical shelf-wave speed of lowest eigenwave versus deep-sea current speed for $\Delta_0 = 1$ and various values of $\varrho' - \varrho$. In the limiting case $\varrho' = \varrho$, the (constant) wave speed is the same as that deduced by Robinson (1964).

order of 100 km) is determined by computing the cross correlation of a few months of daily mean sea-level data from two stations bounding this section, the theory can at most determine average seasonal current speeds in that section or provide the average seasonal difference in the current speed between two widely separated regions (distance separation of the order of 500 km).

The remarkably close agreement between the observed and lowest-mode theoretical wave speeds suggests that the approximations for a nonsloping interface and a semi-infinite width current are reasonable for this theory. The reason for this is that the e-folding distance of the wave amplitude of the surface and interfacial wave in the deep-sea region is $\mu/k\alpha = O(5\times 10^6 \text{ cm})$ for the case of the eastern coast of Australia. In the next section it is shown that, for a current of width l_0, the above results remain essentially unchanged unless $(2k/\mu)l_0 \lesssim 1$.

Solution for Current of Finite Width. Here consideration is given to a stratified model identical to that discussed above except that the deep-sea current is now assumed to lie in the range $l < x < l + l_0$. In this case the eigenvalue equation takes the form (Mysak 1966)

$$\begin{vmatrix} A & B \\ 0 & C \end{vmatrix} = 0, \tag{5.16}$$

where

$$A = \begin{pmatrix} \mathcal{J}_0 & -1 & -1 \\ \Delta_0[(\varkappa)^{1/2}\mathcal{J}_0' + \varkappa\mathcal{J}_0] & -\varkappa + \bar{k}l(1+\varkappa R_0) & -\varkappa - \bar{k}l(1+\varkappa R_0) \\ 0 & -\varkappa R_0 \exp(-\bar{k}l_0) & (2+\varkappa R_0)\exp(\bar{k}l_0) \end{pmatrix}$$

$$B = \begin{pmatrix} -1 & -1 & 0 & 0 \\ -\varkappa + kl(1+\varkappa R_0) & -\varkappa - kl(1+\varkappa R_0) & -1 & 0 \\ 0 & 0 & 0 & 0 \end{pmatrix}$$

$$C = \begin{pmatrix} 1+\omega/f & 1-\omega/f & 0 & 0 \\ -(1+\varkappa R_0)\exp(-kl_0) & (1+\varkappa R_0)\exp(kl_0) & \alpha/\mu & 1 \\ \exp(-kl_0) & \exp(kl_0) & 0 & -1 \\ 0 & 0 & 0 & 1 \end{pmatrix}$$

$0 = 4\times 3$ matrix whose elements are all zero.

In the above, $\mathcal{J}_0$ and $\mathcal{J}_0'$ have the argument $2(\varkappa)^{1/2}$ and $\bar{k} = \alpha k/\mu$. It is well known (Hildebrand 1965: 13) that, if a square matrix M is of the form

$$M = \begin{pmatrix} P & Q \\ O & R \end{pmatrix} \quad \text{or} \quad M = \begin{pmatrix} P & 0 \\ Q & R \end{pmatrix},$$

where P and R are square matrices and where 0 is a submatrix (not necessarily square) whose elements are all zeros, then

$$|M| = |P|\,|R|.$$

Applying this theorem to (5.16), it follows that the eigenvalues are given by $|A| = 0$ and $|C| = 0$. The equation $|C| = 0$, which is a spurious root for our theory, implies that

$$(1 + \omega/f)\exp(kl_0) - (1 - \omega/f)\exp(-kl_0) = 0. \tag{5.17}$$

For $\omega^2 \ll f^2$ and $k^2 l_0^2 \ll 1$, eq. (5.17) implies that $\omega/k = -fl_0$, which, for $l_0 = 10^7$ cm (a typical EAC width) and $f = -0.73 \times 10^{-4}$ sec^{-1}, gives a wave speed of about twice the observed value. The equation $|A| = 0$ implies that

$$\begin{aligned} &\mathcal{J}_0[2(\varkappa)^{1/2}]\{(2 + \varkappa R_0)\exp(\bar{k}l_0)[\varkappa(1 - \Delta_0) - \bar{k}l(1 + \varkappa R_0)] \\ &\quad - \varkappa R_0 \exp(-\bar{k}l_0)[\varkappa(1 - \Delta_0) + (1 + \varkappa R_0)]\} \\ &- \Delta_0(\varkappa)^{1/2}\mathcal{J}_0'[2(\varkappa)^{1/2}][(2 + \varkappa R_0)\exp(\bar{k}l_0) + \varkappa R_0 \exp(-\bar{k}l_0)] = 0. \end{aligned} \tag{5.18}$$

This eigenvalue equation is the generalization of (5.15); as $l_0 \to \infty$, eq. (5.18) reduces to (5.15) upon noting that $\bar{k}l = (\Delta_0)^{1/2}/\beta^*$.

From (5.18) it is clear that the eigenvalues will differ significantly from those obtained in the previous model, only if $\bar{k}l_0 \lesssim 1$, or equivalently, if $l_0 \lesssim [gd_0(\varrho' - \varrho)/\varrho]^{1/2}/|f|$. For $(\varrho' - \varrho)/\varrho = 2.5 \times 10^{-3}$, $d_0 = 2 \times 10^4$ cm, and $|f| = 0.7 \times 10^{-4}$ sec^{-1}, the latter inequality implies that $l_0 \lesssim 3 \times 10^6$ cm. We conclude that this more refined model is required only for a very narrow current. For the EAC, in which $l_0 \approx 10^7$ cm, the current model with semi-infinite width is quite adequate (Fig. 10).

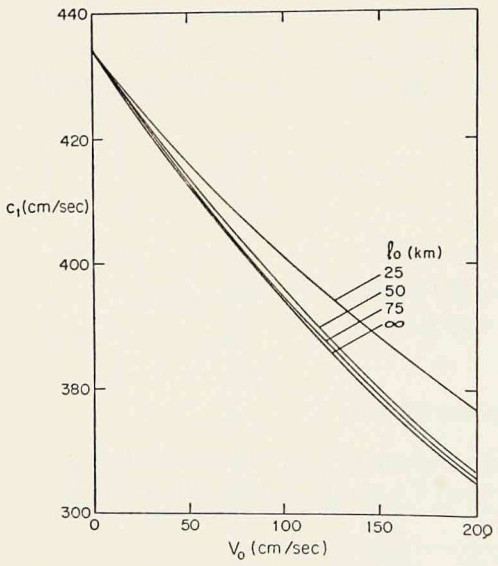

Figure 10. Theoretical shelf-wave speed of lowest eigenwave versus deep-sea current speed for finite and semi-infinite width currents. In each case $\Delta_0 = 1$ and $\varrho' - \varrho = 2.5 \times 10^{-3}$ gm cm^{-3}.

6. *Concluding Remarks.* Although continental shelf waves have so far been observed only on the eastern and western coasts of Australia, it is quite likely that they also exist on other midlatitudinal continental shelves where the coastal and bottom topography is similar to that considered

in this theory.[4] One such region is the eastern United States coastal shelf between Cape Hatteras and Cape Lookout to the south. The shelf in this region is relatively narrow and of constant width; at the edge of the shelf there is a sharp drop to relatively deep water of constant depth. Also, between Cape Hatteras and Cape Lookout, the Florida Current flows northward alongside the edge of the shelf. Therefore it is of considerable interest to apply to this region the theory outlined in § 5 and to thereby calculate the wave speed of the lowest-mode shelf wave as a function of current speed.

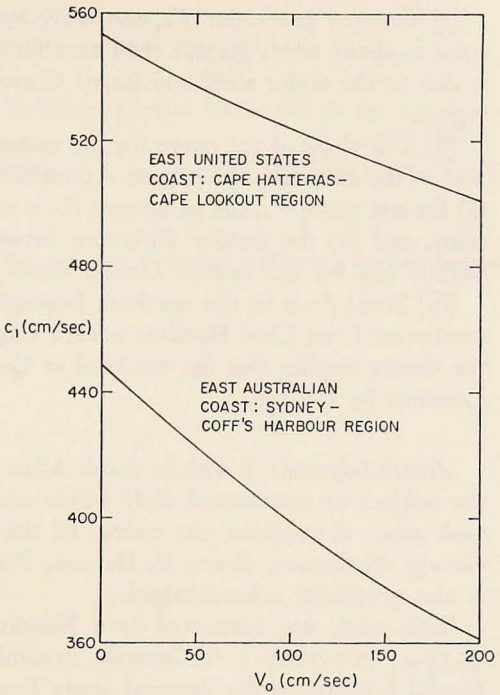

Figure 11. Theoretical shelf-wave speed of lowest eigenwave versus deep-sea current speed for the eastern United States and Australian coasts. In each case $\Delta_0 = 1/2$.

For this region, take $l = 7 \times 10^6$ cm, $d = 2 \times 10^4$ cm, $f = 0.84 \times 10^{-4}$ sec^{-1}, and assume that $\omega = O(10^{-5}$ sec$^{-1})$ and $k = O(2 \times 10^{-8}$ cm$^{-1})$. It then follows that the assumptions $\omega^2 \ll f^2$, $k^2 l^2 \ll 1$, and $f^2 l^2 \ll gd$ also hold for this case, so that the shelf solution derived above is also valid here. Furthermore, since the main portion of the Florida Current in the vicinity of Cape Hatteras is confined to a relatively thin upper layer and is of $O(10^7$ cm) in width, it is justifiable to use the two-layer model with a current of semi-infinite width. Take $\varrho' - \varrho = 2 \times 10^{-3}$ gm cm^{-3}, $d_0 = 4 \times 10^4$ cm, and $D_0 = 4 \times 10^5$ cm. (The interface depth, d_0, can be regarded as an average depth for the 10°C isotherm, which rises from a depth of $7 \times 10^4 - 8 \times 10^4$ cm at 10^7 cm off the shelf to a depth of about 2×10^4 cm at the shelf.) For these values of d_0, D_0, . . ., observe that α and α' are each of order unity and that $\mu^2 \ll 1$, so that the deep-sea solutions derived above are also valid here. Thus it is possible to proceed directly to (5.15) and calculate the lowest eigenvalue as a function of V_0. In Fig. 11 the wave speed of the lowest eigenwave is plotted as a function of current speed for this region and, for comparative purposes, for the region between Sydney and Coff's Harbour.

In Fig. 11, observe the following:

4. And, of course, the region where the waves do exist is likely to be a region of nonbarometric behavior.

(i) For any particular V_0, the wave speed for the eastern United States coast is about 20% greater than that for the eastern Australian coast. This is due to the wider shelf and larger Coriolis parameter in the United States region.

(ii) The slope of the curve for the eastern United States coast is about half that of the curve for the eastern Australian coast. This arises for two reasons: (a) for any given V_0, the paramater R_0 is smaller for the eastern United States coast, and (b) the density difference between the upper and lower layers is slightly less for the eastern United States coast.

(iii) Since $f > 0$ in the northern hemisphere, the shelf waves will progress southward from Cape Hatteras toward Cape Lookout. For $V_0 = 150$ cm/sec, the theory implies that the sea level at Cape Hatteras will lead that at Cape Lookout by 6.8 hrs.

Acknowledgments. I wish to thank Allan R. Robinson for introducing me to the subject of continental shelf waves and for the valuable discussions that took place throughout the course of this work. The helpful assistance of George F. Carrier, Bruce V. Hamon, Peter H. Stone, and Pearn P. Niiler is also gratefully acknowledged.

This work was supported by a National Science Foundation Grant GP 3533-44-709-7869-2 in oceanic dynamics to Harvard University and a Special Scholarship for doctoral study from the National Research Council of Canada.

REFERENCES

CSIRO Australia
1963. Oceanographic Cruise Rep., 6; 115 pp.

Greenspan, H. P.
1956. The generation of edgewaves by moving pressure distributions. J. fluid Mech., *1*: 574–592.

Hamon, B. V.
1962. The spectrums of mean sea level at Sydney, Coff's Harbour, and Lord Howe Island. J. geophys. Res., *67*: 5147–5155.
1963. Correction to "The spectrums of mean sea level at Sydney, Coff's Harbour, and Lord Howe Island". J. geophys. Res., *68*: 4635.
1965. The east Australian current, 1960–1964. Deep-sea Res., *12*: 899–922.
1966. Continental shelf waves and the effects of atmospheric pressure and wind stress on sea level. J. geophys. Res., *71*: 2883–2896.

Hamon, B. V., and E. J. Hannan
1963. Estimating relations between time series. J. geophys. Res., *68*: 6033–6041.

Hildebrand, F. B.
1965. Methods of applied mathematics. 2nd edition. Prentice-Hall, Inc., New York. 362 pp.

MUNK, W. H., F. E. SNODGRASS, and G. F. CARRIER
1956. Edgewaves on the continental shelf. Science, *123*: 127–132.

MYSAK, L. A.
1966. Continental shelf waves, Ph. D. Thesis, Harvard University. 69 pp.

REID, R. O.
1958. Effect of Coriolis force on edgewaves. I. Investigation of normal modes. J. mar. Res., *16*: 109–144.

ROBINSON, A. R.
1964. Continental shelf waves and the response of the sea surface to weather systems. J. geophys. Res., *69*: 367–368.